BIOLOGICAL CRYSTALLOGRAPHY

ISSN 1399-0047

Enantioselective oxidation of galactitol 1-phosphate by galactitol-1-phosphate 5-dehydrogenase from *Escherichia coli*

Rocío Benavente,[a]‡ María Esteban-Torres,[b]§‡ Gert-Wieland Kohring,[c] Álvaro Cortés-Cabrera,[d] Pedro A. Sánchez-Murcia,[d] Federico Gago,[d] Iván Acebrón,[a] Blanca de las Rivas,[b] Rosario Muñoz[b] and José M. Mancheño[a]*

[a]Department of Crystallography and Structural Biology, Institute of Physical Chemistry Rocasolano, CSIC, Serrano 119, 28006 Madrid, Spain, [b]Laboratory of Bacterial Biotechnology, Institute of Food Science and Technology and Nutrition (ICTAN), CSIC, Juan de la Cierva 3, 28006 Madrid, Spain, [c]Microbiology, Saarland University, Campus Gebäude A1.5, 66123 Saarbruecken, Germany, and [d]Department of Biomedical Sciences, School of Medicine and Health Sciences, University of Alcalá, 28871 Alcalá de Henares, Spain. *Correspondence e-mail: xjosemi@iqfr.csic.es

Received 2 March 2015
Accepted 15 May 2015

Edited by Z. S. Derewenda, University of Virginia, USA

‡ These authors contributed equally to this work.
§ Current address: Alimentary Pharmabiotic Centre and Department of Microbiology, Bioscience Institute, National University of Ireland, Western Road, Cork, Ireland.

Keywords: crystal structure; galactitol-1-phosphate 5-dehydrogenase; metal binding; enantioselectivity; galactitol phosphate; dehydrogenase; metal coordination; catalytic mechanism.

PDB references: GPDH–Zn^{2+}, 4ueo; GPDH–Zn^{2+}–Tris, 4uek; GPDH–Zn^{2+}–glycerol, 4uej

Supporting information: this article has supporting information at journals.iucr.org/d

Galactitol-1-phosphate 5-dehydrogenase (GPDH) is a polyol dehydrogenase that belongs to the medium-chain dehydrogenase/reductase (MDR) superfamily. It catalyses the Zn^{2+}- and NAD^+-dependent stereoselective dehydrogenation of L-galactitol 1-phosphate to D-tagatose 6-phosphate. Here, three crystal structures of GPDH from *Escherichia coli* are reported: that of the open state of GPDH with Zn^{2+} in the catalytic site and those of the closed state in complex with the polyols Tris and glycerol, respectively. The closed state of GPDH reveals no bound cofactor, which is at variance with the conformational transition of the prototypical mammalian liver alcohol dehydrogenase. The main intersubunit-contacting interface within the GPDH homodimer presents a large internal cavity that probably facilitates the relative movement between the subunits. The substrate analogue glycerol bound within the active site partially mimics the catalytically relevant backbone of galactitol 1-phosphate. The glycerol binding mode reveals, for the first time in the polyol dehydrogenases, a pentacoordinated zinc ion in complex with a polyol and also a strong hydrogen bond between the primary hydroxyl group and the conserved Glu144, an interaction originally proposed more than thirty years ago that supports a catalytic role for this acidic residue.

1. Introduction

The superfamily of medium-chain dehydrogenase/reductase (MDR) enzymes catalyse the reversible oxidation of primary and secondary alcohols to aldehydes and ketones, respectively, using NAD(P) as a cofactor (Persson *et al.*, 2008). These enzymes comprise a group of different Zn^{2+}-dependent alcohol dehydrogenases (ADHs; EC 1.1.1.1), historically typified by yeast and liver ADHs (Riveros-Rosas *et al.*, 2003). The polyol dehydrogenases (PDHs) form a distinct family that includes sorbitol dehydrogenase (SDH; EC 1.1.1.14; Jeffery & Jörnvall, 1988), xylitol dehydrogenase (EC 1.1.1.9; Persson *et al.*, 1994) and galactitol-1-phosphate 5-dehydrogenase (GPDH; EC 1.1.1.251; Nobelmann & Lengeler, 1995), among many others.

Currently, the structures of many MDR enzymes have been solved (Eklund & Ramaswamy, 2008). Basically, all members share a common subunit architecture that is constructed from two domains: a catalytic domain and a nucleotide-binding domain. Between them there is a deep cleft that hosts the catalytically requisite Zn^{2+} ion and the cofactor. These protein

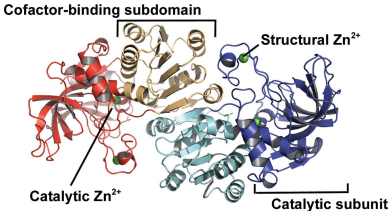

subunits associate into homodimeric assemblies in mammalian ADHs or into homotetramers in fungal, bacterial and yeast ADHs (Eklund & Ramaswamy, 2008) and also in PDHs (Klimacek *et al.*, 2007). Together with the catalytic zinc ion, most dehydrogenases from this superfamily have another zinc which is also located in the catalytic domain, specifically within the so-called lobe loop, which is defined as the structural zinc (Auld & Bergman, 2008) and whose functional role, if any, is not yet clear (Raj *et al.*, 2014). Interestingly, functional tetrameric PDHs lack this structural zinc; hence, they contain only one metal per subunit (Jeffery & Jörnvall, 1988).

Whereas the coordination of structural zinc ions by four cysteine residues is, with some exceptions (Guy *et al.*, 2003; Pennacchio *et al.*, 2009), essentially conserved (Auld & Bergman, 2008; Raj *et al.*, 2014), the coordination of catalytic zinc ions is much less homogeneous and is currently under intense investigation with regard to both the participating ligands and the potential changes occurring in the catalytic cycle that would affect the coordination number of the zinc ion (tetracoordinated and pentacoordinated) or the zinc–ligand bond distances (Ryde, 1995; Baker *et al.*, 2009). Obviously, elucidation of these latter dynamic aspects is relevant to the wider MDR superfamily since they are intimately connected to the structural basis of catalysis by these enzymes. In this regard, uncertainties remain about the functional roles of the acidic residues Glu60 (using GPDH numbering) and Glu144, both of which are conserved among the PDHs (Eklund *et al.*, 1985; Jeffery & Jörnvall, 1988) and which are very close to the catalytic zinc. Whereas in this latter family of enzymes Glu60 (Glu68 in horse liver ADH; hlADH) is a ligand of Zn^{2+} (Klimacek *et al.*, 2007), Glu144 (Cys174 in hlADH) is linked to the zinc ion through a water molecule (also conserved in the family) and thus belongs to the second coordination sphere. In the case of hlADH, Glu68, which does not coordinate to the metal in the absence of substrates (the ligands of the zinc are Cys46, His67, Cys174 and a water molecule), has been suggested to play different roles, namely a stabilizing role in the active site (Al-Karadaghi *et al.*, 1994), as a modulator of the electrostatic field in this environment (Ganzhorn & Plapp, 1988) and also as a transient ligand of the zinc during the catalytic cycle, permitting efficient product release (Ryde, 1995). In other cases, however, substitution of this residue by an alanine or an aspartic acid has minor effects on catalysis (Kleifeld, 2003).

Regarding Glu144, Eklund *et al.* (1985) originally proposed that this residue would be involved in substrate binding in PDHs by specifically forming a strong hydrogen bond to the primary hydroxyl group adjacent to the secondary hydroxyl group undergoing reaction. Despite a lack of direct structural evidence supporting this idea, the crystal structure of human sorbitol dehydrogenase (SDH) in complex with NADH and the inhibitor CP-166,572 (PDB entry 1pl6) is consistent with this hypothesis, revealing a 2.4 Å hydrogen bond between the side chain of Glu144 (Glu155 in SDH) and the primary hydroxyl group of the inhibitor (Pauly *et al.*, 2003). Moreover, kinetic isotope effect studies with xylitol dehydrogenase from the yeast *Galactocandida mastotermitis* identified a role for this residue as a modulator of general base catalysis, not being essential for hydrogen transfer (Klimacek *et al.*, 2007).

Conversely, catalysis by hlADH is intimately linked to conformational flexibility, and in fact this protein was one of the first enzymes for which different conformational states were reported for the apo and holo forms (Brändén, 1965). Nevertheless, despite our current knowledge about these conformational changes (Plapp, 2010), the connections between protein dynamics and catalysis are not well understood. Basically, the main conformational features in hlADH that have been identified during catalysis are a global conformational change affecting the relative orientation of the catalytic and cofactor-binding domains that occurs upon binding of the coenzyme, and loop rearrangements around residues 292–299 of the coenzyme-binding domain. Other minor changes affecting the active site result from the exchange of zinc ligands, perhaps involving pentacoordinated zinc intermediates (Dworschack & Plapp, 1977; Makinen & Yim, 1981). The predominant scenario explaining these conformational changes is that of an induced fit; namely, the enzyme changes conformation upon the binding of substrates (Plapp, 2010) and, specifically for hlADH, it has been shown that binding of the complete coenzyme is required for the transition between the open state (apo form) and the closed state (holo form) (Eklund & Ramaswamy, 2008). Nevertheless, it is not clear that this transition is required for catalysis because the catalytic residues occupy similar positions in both forms; in this regard, only minor changes have been observed between the apo and holo forms in human SDH (Pauly *et al.*, 2003).

The crystal structures of GPDH that we report in this work offer novel details of the PDH family with respect to several enzymatic issues that may be relevant to the wider MDR superfamily. Thus, the structure of the apo form reveals that, in contrast to the currently known crystal structures of PDHs, GPDH has a structural Zn^{2+} per subunit in addition to the catalytic metal ion. Furthermore, the structure of the closed state obtained in complex with the substrate analogue glycerol reveals key structural features: for the first time the Zn^{2+} is observed pentacoordinated with a polyol that is structurally homologous to the catalytically relevant part of the substrate; secondly, also at variance with PDHs, Glu60 is not a ligand of the Zn^{2+}; and, thirdly, this complex reveals the originally predicted strong hydrogen bond between the primary alcohol and Glu144 while the secondary alcohol is directly coordinating the Zn^{2+}. Finally, it is remarkable that the closed state of GPDH is observed with substrate analogues lodged within the active site but in the absence of bound cofactor.

2. Materials and methods

2.1. DNA manipulations

The expression vector pT77-GPDH coding for the wild-type galactitol-1-phosphate 5-dehydrogenase from *Escherichia coli* K12 (Esteban-Torres *et al.*, 2012) was used as template for the preparation of single-point variants affecting residues located

in the active-site region of GPDH (Ser40, Arg44, His51, Tyr106 and Arg112) by site-directed mutagenesis PCR. The mutagenic primers used (forward and reverse, respectively) were S40A-fw (5′-GCTTATGTGGTGCCGATTTACC-3′) and S40A-rv (5′-GGTAAATCGGCACCACATAAGC-3′) for the Ser40Ala variant, R44T-fw (5′-CGATTTACCCACCATATTTAAAAATGG-3′) and R44T-rv (5′-CCATTTTTAAATATGGTGGGTAAATCG-3′) for the Arg44Thr variant, H51A-fw (5′-GGTGCAGCTTATTATCC-3′) and H51A-rv (5′-GGATAATAAGCTGCACC-3′) for the His51Ala variant, Y106A-fw (5′-GTGCGCAAAAGCTGATTTTATTGG-3′) and Y106A-rv (5′-CCAATAAAATCAGCTTTTGCGCAC-3′) for the Tyr106Ala variant and, finally, R112A-fw (5′-GGCTCAGCGCGTGATGGTGGATTTG-3′) and R112A-rv (5′-AATCCACCATCACGCGCTGAGCC-3′) for the Arg112Ala variant. The mutated GPDH genes were sequenced to verify the expected nucleotide changes.

2.2. Protein expression and purification

Wild-type and single-point mutants of GPDH were produced and purified essentially as described previously (Esteban-Torres *et al.*, 2012). Briefly, cells carrying the corresponding recombinant plasmid were grown at 37°C in LB medium containing ampicillin (100 µg ml^{-1}) and induced by adding 0.4 m*M* isopropyl *β*-D-1-thiogalactopyranoside. After induction, the cells were grown at 22°C for 20 h and were collected by centrifugation using a Beckman Coulter J-25 Avanti centrifuge (7500*g* for 15 min at 4°C). The cells were resuspended in 20 ml 20 m*M* Tris–HCl pH 8.0 containing 100 m*M* NaCl per litre of cell culture. Crude extracts were prepared by French press lysis of cell suspensions. The lysate was centrifuged at 17 400*g* for 40 min at 4°C using a Beckman Coulter J-25 Avanti centrifuge. The supernatant was filtered through a 0.22 µm filter (Millipore) and subsequently loaded onto a HisTrap FF column (GE Healthcare) previously equilibrated in binding buffer (20 m*M* Tris–HCl pH 8.0 containing 100 m*M* NaCl and 10 m*M* imidazole). The recombinant proteins were eluted with a linear gradient of imidazole (from 10 to 500 m*M*) with an ÄKTAprime plus. Fractions containing the target protein were pooled and concentrated by ultrafiltration. The protein (2 ml) was then loaded onto a HiTrap Q HP ion-exchange column (GE Healthcare) equilibrated in 20 m*M* Tris–HCl pH 8.0 containing 10 m*M* NaCl. Elution of the proteins was carried out with a linear gradient of sodium chloride (from 10 to 500 m*M*). As before, fractions containing the target protein were pooled and concentrated by ultrafiltration. The final purified material was stored at −80°C until use.

The preparation of the GPDH–Zn^{2+} binary complex was performed as follows. Firstly, wild-type GPDH (10 mg ml^{-1}) in Tris buffer pH 8.0 (20 m*M* Tris–HCl pH 8.0, 100 m*M* NaCl) was buffer-exchanged into zinc-containing buffer (20 m*M* Tris–HCl pH 9.0, 100 m*M* NaCl, 0.5 m*M* zinc chloride) using a HiTrap desalting column (GE Healthcare). The eluted protein was concentrated to 12 mg ml^{-1} for crystallization trials or used as a starting material for preparation of the tertiary complex GPDH–Zn^{2+}–NAD^+. In this case, NADH was added to the protein solution to a final concentration of 1.8 m*M* and incubated overnight at 4°C. The mixture was then concentrated and loaded onto a HiTrap desalting column (GE Healthcare) equilibrated in Tris buffer pH 8.0. The eluted protein was concentrated to 12 mg ml^{-1} for crystallization trials. UV–Vis absorbance scans of this protein stock solution showed a maximum at 340 nm, indicating the presence of NADH.

2.3. Synthesis of galactitol 1-phosphate and activity assays

L-Galactitol 1-phosphate (LG1P) and D-galactitol 1-phosphate (DG1P) were synthesized and verified by Elexopharm, Saarbruecken, Germany (http://www.elexopharm.de). All enzymatic tests were performed in duplicate. Catalytic constants for the oxidation of LG1P were determined in 100 m*M* Tris–HCl buffer pH 9.0 containing 0.5 m*M* $ZnCl_2$, 1.8 m*M* NAD^+ and concentrations of GPDH variants between 4 and 50 µg ml^{-1}. The reaction was started by addition of the substrate and the change in extinction was followed at 340 nm using an Ultrospec 2100 pro photometer (GE Healthcare). For inhibition experiments, 1 or 3 m*M* DG1P was added to the buffer prior to starting the reaction with LG1P.

Protein concentrations were determined using the BCA Protein Assay kit (Pierce) with bovine serum albumin as the standard (Smith *et al.*, 1985).

2.4. Crystallization

Whereas GPDH incubated with Zn^{2+} crystallized under the same experimental conditions as described previously (Esteban-Torres *et al.*, 2012), conditions for crystallization of GPDH incubated with Zn^{2+} and NAD(H) were determined *de novo* by the sitting-drop vapour-diffusion method using commercial screens from Hampton Research (Riverside, California, USA) and Qiagen in Innovaplate SD-2 96-well plates set up using an Innovadyne Nanodrop robot. Each drop consisted of 250 nl protein solution (12 mg ml^{-1}) in Tris–HCl buffer (20 m*M* Tris–HCl pH 8.0 containing 0.1 *M* NaCl) and 250 nl reservoir solution. Drops were equilibrated against 65 µl reservoir solution. Initial crystals were observed in 20%(*w*/*v*) PEG 6000, 0.1 *M* Tris–HCl pH 8.0, 0.2 *M* $CaCl_2$ and also in 15%(*w*/*v*) PEG 4000, 0.1 *M* Tris–HCl pH 8.5, 0.2 *M* magnesium chloride. After scaling up and optimization of the crystallization conditions using hanging drops in 24-well VDX plates, high-quality diffracting crystals were prepared in 16%(*w*/*v*) PEG 4000, 0.2 *M* magnesium chloride, 0.1 *M* Tris–HCl pH 8.5 (2:1 protein:precipitant volume ratio; total volume 3 µl). Crystallization trials of GPDH incubated with Zn^{2+} using NAD(H) as an additive (1–10 m*M* concentration range) were also attempted but were unsuccessful. Similar experiments carried out with NAD^+ were also unsuccessful.

2.5. Data collection, processing and structure solution

Crystals suitable for X-ray analysis were transferred into an optimized cryoprotectant solution [reservoir solution plus 20%(*v*/*v*) glycerol] for ∼5–10 s (2 min for the crystal measured

on beamline ID23-1) and then cryocooled to 100 K in a cold nitrogen-gas stream. To avoid potential backsoaking of the coenzyme from crystals of GPDH incubated with Zn^{2+} and NAD(H), the cryoprotectant solution was prepared with NAD(H) (1–10 m*M*); however, under these conditions the crystals were rapidly damaged. Hence, backsoaking cannot be discarded. Diffraction data from crystals of GPDH pre-incubated with Zn^{2+} were recorded on the BL13-XALOC beamline at the ALBA synchrotron, Barcelona, Spain at the zinc peak (9.667 keV; 1.28245 Å wavelength) as determined experimentally from the corresponding fluorescence energy scan. A Pilatus 6M detector (Area Detector Systems Corp.) was used at a crystal-to-detector distance of 268.14 mm, and a total of 360 images were collected with a 0.5° oscillation angle. Additionally, two data sets from crystals prepared from GPDH pre-incubated with Zn^{2+} and NADH were collected on beamlines ID29 and ID23-1 at the ESRF, Grenoble, France using wavelengths of 1.28149 and 0.96885 Å, respectively. Whereas the crystal measured on beamline ID29 was incubated for ∼5–10 s in the cryoprotectant solution, that measured on ID23-1 was incubated for ∼2 min. In both cases a Pilatus 6M detector was used. A total of 3600 images were collected on beamline ID29 with a 0.10° oscillation angle and a crystal-to-detector distance of 317.48 mm. The data set collected on beamline ID23-1 consisted of 2400 images collected with an oscillation angle of 0.15° and a crystal-to-detector distance of 188.84 mm. Diffraction images were processed with the *XDS* (Kabsch, 2010) program package. Space-group examination was performed with *POINTLESS* (Evans, 2011) and reduction of intensities was performed with *AIMLESS* (Evans, 2011) from the *CCP*4 suite of programs (Winn *et al.*, 2011). The first crystal form (GPDH incubated with Zn^{2+} only) belonged to the monoclinic space group $P2_1$, with unit-cell parameters a = 43.31, b = 76.91, c = 108.65 Å, β = 95.51°, and is defined here as crystal form I. The crystals obtained from GPDH pre-incubated with Zn^{2+} and NADH were also monoclinic (space group $P2_1$), with unit-cell parameters a = 65.31, b = 78.81, c = 68.24 Å, β = 94.75°, and are defined as crystal form II. Data statistics are summarized in Table 1.

Table 1
Data-collection and refinement statistics for GPDH structures.

Values in parentheses are for the last shell.

	GPDH–Zn^{2+} (model 1)	GPDH–Zn^{2+}–Tris (model 2)	GPDH–Zn^{2+}–glycerol (model 3)
Data statistics			
Beamline	BL13-XALOC	ID29	ID23-1
Wavelength (Å)	1.2824	1.2815	0.9688
Space group	$P2_1$	$P2_1$	$P2_1$
a, b, c (Å)	43.3, 76.9, 108.6	65.6, 78.9, 68.6	65.3, 78.8, 68.2
α, β, γ (°)	90.0, 95.5, 90.0	90.0, 94.6, 90.0	90.0, 94.7, 90.0
Resolution (Å)	2.0	1.9	1.7
Completeness (%)	97.8 (96.0)	89.7 (54.7)	99.2 (98.7)
No. of observed reflections	160822	299907	483893
No. of unique reflections	47058	49264	70089
$R_{p.i.m.}$† (%)	4.3 (41.1)	5.1 (29.6)	4.0 (25.3)
$\langle I/\sigma(I)\rangle$	8.7 (1.8)	7.9 (2.3)	11.2 (3.2)
Wilson B factor (Å^2)	31.3	11.9	15.4
Refinement statistics			
Resolution limits (Å)	44.2–2.0	45.2–1.9	41.7–1.7
Z	2	2	2
No. of reflections used	44566	46624	66417
R_{cryst}‡ (%)	19.5	20.2	18.5
R_{free}§ (%)	25.6	25.8	22.8
No. of atoms			
Protein	5254	5270	5349
Ligands	5	7	7
Water	276	471	654
Average B factor (Å^2)			
Protein			
Chain A	50.7	22.8	23.6
Chain B	60.9	24.6	19.5
Ligands			
Zn^{2+}	85.5	27.9	18.6
Tris	—	30.2	—
Glycerol	—	—	31.1
Water oxygen	49.7	32.4	33.2
R.m.s.d., bond lengths (Å)	0.009	0.008	0.007
R.m.s.d., bond angles (°)	1.28	1.16	1.11
Ramachandran plot			
Favoured (%)	91.7	97.1	96.9
Allowed (%)	6.4	2.9	2.9
Outliers (%)	1.9	0	0.2
PDB code	4ueo	4uek	4uej

† $R_{p.i.m.} = \sum_{hkl}\{1/[N(hkl)-1]\}^{1/2}\sum_i |I_i(hkl) - \langle I(hkl)\rangle|/\sum_{hkl}\sum_i I_i(hkl)$. ‡ $R_{cryst} = \sum_{hkl}\big||F_{obs}| - |F_{calc}|\big|/\sum_{hkl}|F_{obs}|$. § R_{free} is the cross-validation R factor for the 5% of the reflections against which the model was not refined.

2.6. Structure determination and refinement

The crystal structure was determined by molecular replacement using *Phaser* (McCoy *et al.*, 2007). The atomic coordinates of GPDH (PDB entry 4a2c; Esteban-Torres *et al.*, 2012) were used as a search model. Model rebuilding was performed manually using *Coot* (Emsley *et al.*, 2010) and refinement was performed with *phenix.refine* (Afonine *et al.*, 2012) in *PHENIX* (Adams *et al.*, 2010). Refinement steps included *xyz* refinement, TLS, individual atomic displacement parameters (ADPs), addition of ligands and automatic addition of water molecules using default parameters. Stereochemical validation was carried out using *MolProbity* (Chen *et al.*, 2010). The refinement statistics shown in Table 1 show that the quality of the GPDH–Zn^{2+} complex model (PDB entry 4ueo) is lower than that of the other two models. In fact, whereas all of the residues in the latter two models were defined in the electron-density map, no density was observed in three loops of the GPDH–Zn^{2+} complex (specifically residues 6–12, 41–56 and 334–338). *PyMOL* (DeLano, 2008) was used for structure visualization, figure preparation and molecular editing.

2.7. Computational methods

To account for substrate and cofactor recognition, the three-dimensional coordinates of the enzyme structure in the apo form were used to build a model of the Michaelis complex. Initial positions for the NAD^+ cofactor and the catalytic zinc ion were obtained from the best-fit superimposition of this apo form onto *Neurospora crassa* L-arabinitol-4-dehydrogenase (PDB entry 3m6i; Bae *et al.*, 2010) using the structural alignment tool implemented in *PyMOL*. The location of the

cofactor was compared with that found in other related dehydrogenases from the same MDR superfamily and it was established that the key ligand–protein interactions were present. The geometry of the resulting complex was optimized by following an energy-minimization protocol consisting of 2000 steps of steepest descent followed by 3000 steps of conjugate gradient. The Amber 10 force field and published parameters for NAD^+ (Ryde, 1995) were employed. To place the LG1P and DG1P molecules inside the active site of the modelled enzyme, we used our in-house *CRDOCK* docking program (Cortés Cabrera *et al.*, 2012) and default parameters. The binding poses obtained for each molecule were ranked according to the calculated interaction energies but also taking into account the feasibility of the enzymatic reaction on the basis of the distances separating C5 of LG1P from C4 of the NAD^+ molecule (≤4.0 Å) and the O5 and O6 atoms from the zinc ion (≤2.5 Å). By following this procedure, we were able to select the most likely binding orientations for both substrates within the enzyme active site.

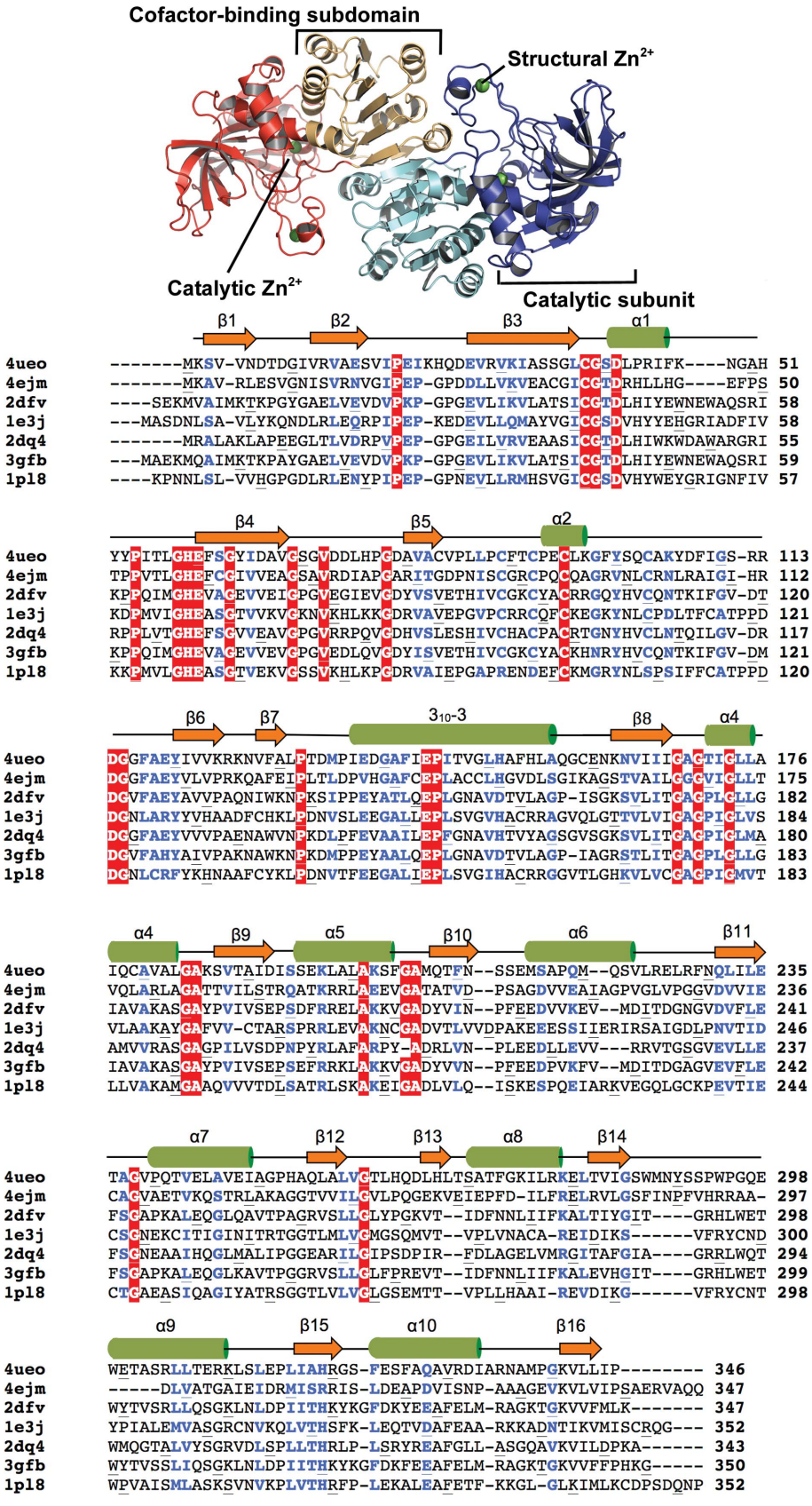

2.8. PDB accession codes

Atomic coordinates and structure-factor amplitudes have been deposited in the Protein Data Bank and are available under the accession codes 4ueo (open state of GPDH with Zn^{2+} in the catalytic site), 4uej (closed state of GPDH with glycerol in the active site) and 4uek (closed state of GPDH with Tris in the active site).

Figure 1
Multiple amino-acid sequence alignment of GPDH with the closest structural homologues: zinc-binding dehydrogenase from *S. meliloti* (PDB entry 4ejm), threonine dehydrogenase from *P. horikoshii* (PDB entry 2dfv), sorbitol dehydrogenase from silverleaf whitefly (PDB entry 1e3j), threonine 3-dehydrogenase from *T. thermophilus* (PDB entry 2dq4), L-threonine dehydrogenase from *T. kodakaraensis* (PDB entry 3gfb) and human sorbitol dehydrogenase (PDB entry 1pl8). Secondary-structural elements of GPDH according to *DSSP* are indicated as orange arrows (β-strands) and green cylinders (α-helices). In the upper part an overall view of GPDH (represented as ribbon model) is shown indicating the locations of the catalytic and the structural zincs (green spheres) and the relative orientation of the GPDH subdomains.

3. Results and discussion

3.1. Overall structure of the GPDH monomer: some comments about the two GPDH crystal forms obtained

Two different monoclinic crystals of GPDH have been prepared in this work. Crystal form I is defined here as that corresponding to crystals of GPDH that have not been incubated with NADH; it contains either nickel scavenged during purification (Esteban-Torres *et al.*, 2012) or externally added zinc (this work; PDB entry 4ueo) in the catalytic metal-binding site. Conversely, crystal form II corresponds to crystals of GPDH that have been incubated with Zn^{2+} and NADH [this work; PDB entries 4uek (model 2) and 4uej (model 3)]. Despite the fact that these latter incubation conditions permitted the reconstruction of the holoenzyme in solution, as revealed spectroscopically (not shown), no electron density assignable to the cofactor was observed. Comparison of the structure of GPDH in crystal form II (either model 2 or 3) with that in crystal form I (model 1) reveals a global conformational change in GPDH, similar to the classical conformational change undergone by horse liver ADH (hlADH) upon cofactor binding (Eklund *et al.*, 1981). This conformational change mainly involves a relative reorientation of the two subdomains of the protein subunits (see below) and therefore does not affect the description of the overall structure of the GPDH subunits. For this, we have arbitrarily chosen molecule *A* from crystal form II (the subunit conformations of models 2 and 3 are essentially indistinguishable) as a reference.

The GPDH monomer comprises 346 amino-acid residues arranged in two distinct subdomains, as typically observed in the members of the MDR superfamily (Eklund & Ramaswamy, 2008): a discontinuous, large catalytic domain (residues 1–148 and 286–346) and a smaller cofactor-binding domain (residues 149–285) (Fig. 1). The subdomains are separated by a deep cleft in which the active site is located and therefore in which the NAD(H) cofactor, the catalytic zinc and the substrates are accommodated (Eklund & Ramaswamy, 2008). The cofactor-binding domain is a canonical Rossmann fold characteristic of NAD(H)-binding proteins (Bellamacina, 1996; Fan & Plapp, 1999), which is made up of a six-stranded parallel β-sheet surrounded by α-helices.

The core of the catalytic domain is formed by a seven-stranded mixed β-sheet [five antiparallel (β3, β4, β5, β6 and β7) and two parallel (β15, β16) β-strands], which is flanked by a two-stranded antiparallel β-sheet (β1 and β2) and three α-helices (α1, 3_{10}-3 and α10). The main contacting regions between these two subdomains arise from the loop that houses the structural zinc-binding site (lobe loop), which interacts with two connecting loops from the other subdomain (the loop between strand β14 and helix α9 and the loop between helices 3_{10}-3 and α4). As also observed in other members of the MDR superfamily, a distinct kink is present within the 3_{10}-3 helix preceding the position of the functionally relevant Glu144 (see below).

Two bound metal ions per GPDH subunit are identified in both crystal forms, which are here unambiguously identified as zinc by the use of diffraction data collected at the Zn peak (see below). This observation agrees with the fact that most NAD(H)-dependent dehydrogenases from the MDR superfamily have two zinc ions per subunit (Auld & Bergman, 2008), namely one catalytic zinc within the active site and another one located in the lobe loop of the catalytic subdomain, but it is at variance with the known structures of functional, tetrameric PDH enzymes, which lack the structural zinc (Jeffery & Jörnvall, 1988). In contrast to this, in some bacterial MDR alcohol dehydrogenases this zinc-containing loop has been shown to be important for tetramer formation (Banfield *et al.*, 2001; Esposito *et al.*, 2002; Guy *et al.*, 2003). Thus, GPDH is a peculiar PDH insofar as it is dimeric and contains two zincs per subunit. In fact, we found that bacterial, dimeric MDR enzymes are reductases but lack zinc ions (Edwards *et al.*, 1996; Shimomura *et al.*, 2003; Sulzenbacher, Roig-Zamboni *et al.*, 2004).

As expected, matching a GPDH subunit against the PDB using the *DALI* server (Holm & Sander, 1995) revealed that the closest structural homologues are ADH and PDH enzymes from the MDR superfamily, in particular a putative zinc-binding dehydrogenase from *Sinorhizobium meliloti* (PDB entry 4ejm; r.m.s.d. of 2.0 Å for 332 C^{α} atoms; New York Structural Genomics Research Consortium, unpublished work), L-threonine dehydrogenase from *Pyrococcus horikoshii* (PDB entry 2dfv; r.m.s.d. of 1.9 Å for 331 C^{α} atoms; Ishikawa *et al.*, 2007), ketose reductase (sorbitol dehydrogenase) from silverleaf whitefly (PDB entry 1e3j; r.m.s.d. of 1.9 Å for 331 C^{α} atoms; Banfield *et al.*, 2001), L-threonine 3-dehydrogenase from *Thermus thermophilus* (PDB entry 2dq4; r.m.s.d. of 2.0 Å for 336 C^{α} atoms; RIKEN Structural Genomics/Proteomics Initiative, unpublished work), L-threonine dehydrogenase from *Thermococcus kodakaraensis* (PDB entry 3gfb; r.m.s.d. of 2.0 Å for 334 C^{α} atoms; Bowyer *et al.*, 2009), human sorbitol dehydrogenase (hSDH; PDB entry 1pl8; r.m.s.d. of 2.1 Å for 335 C^{α} atoms; Pauly *et al.*, 2003) and also many other ADHs with r.m.s.d. values around 2 Å. The result reveals a remarkably high degree of conservation of the architecture of the protein subunits despite the low level of sequence identity among them (less than 27%; Fig. 1).

3.2. Quaternary structure of GPDH and the build-up of an internal cavity

In contrast to bacterial ADHs and PDH enzymes, which are tetrameric assemblies, GPDH is a dimer both in solution and in the crystal (Esteban-Torres *et al.*, 2012). The association between GPDH subunits occurs through their cofactor-binding subdomains. The main contacting interface buries approximately 3450 $Å^2$ per dimer and results from contacts between the β12–β13 connecting loop, strands β13 and β14 and helix α8 from each subunit. It is remarkable that upon dimer formation these structural elements, together with helix α7 and strand β12 from each subunit, delimit an internal, large solvent-inaccessible cavity (310 $Å^3$ in volume as estimated by the *CASTp* server; Dundas *et al.*, 2006; Figs. 2*a* and 2*b*) lined exclusively with hydrophobic residues (Val243, Val247, Leu256, Leu258, Leu266, Leu268, Phe273, Ile276 and Val283;

Fig. 2*c*). As can be seen in Fig. 2, the structural elements forming the cavity are related by a noncrystallographic twofold axis. The overall shape of this cavity is that of a rectangular prism: one of its sides is surrounded by the two-stranded, intersubunit, antiparallel β-sheet formed by strands β13, whereas the opposite side is defined by strands β12 and β14 from each subunit. One pair of perpendicular and opposed faces of the cavity is formed by helix α8 from one subunit and the β12–β13 connecting loop from the other subunit, whereas the other opposed pair of faces is defined by helices α7. As far as we know, similar cavities have not been described previously for any other enzyme from the MDR superfamily, irrespective of the highly conserved protein architecture of these proteins. On the contrary, all of the structural homologues found for GPDH have tightly packed hydrophobic cores in the equivalent regions.

As expected from their crucial location at the intersubunit-contacting interface, structural elements of GPDH exist that probably contribute to stabilizing the dimeric assembly. In particular, helix α8 (residues 270–278) is an important intersubunit secondary-structure element, together with strands β12 and β14. This helix participates in several intersubunit contacts: (i) a cation–π interaction between Arg278 and Trp287, (ii) a salt bridge between Glu280 and His151 (2.3 Å) and (iii) a hydrophobic cluster formed by Phe273 and Leu277 on the one hand and residues Val243, Leu258 and Leu262 from the contacting subunit on the other. We believe that in contrast to these intersubunit-stabilizing interactions, the presence of a large, internal cavity at the intersubunit interface should be considered *a priori* as a destabilizing factor essentially owing to the inefficient packing of hydrophobic side chains. In fact, it is well known that cavity-creating mutations within hydrophobic cores in proteins are generally destabilizing (Eriksson *et al.*, 1992; Jackson *et al.*, 1993; Buckle *et al.*, 1996).

Although the electron-density map does not reveal any ordered water molecule within the cavity, which is in agreement with the low probability of finding a single water molecule in a small hydrophobic cavity (1 in 20 000; Wolfenden & Radzicka, 1994), the existence of water molecules in large hydrophobic cavities in proteins is contentious (Matthews *et al.*, 1995), perhaps because of the assumption that a lack of density in a crystallographic electron-density map means an absence of matter (Yu *et al.*, 1999). Although these maps do not usually reveal any atoms whose average position is ill-defined, a large body of studies on hydrogen exchange show that solvent can penetrate deep into the protein structure (Englander & Kallenbach, 1983). For this reason, we think that it is reasonable to propose the existence of mobile solvent within the observed cavity of GPDH which may play a role in protein dynamics. In this regard, in this work we have identified two distinct conformational states of GPDH (open and closed states, respectively), which are similar to those originally identified in hlADH (Eklund *et al.*, 1981). Comparison between these two conformational states reveals the displacement of side chains facing the cavity, which most probably occurs in synchrony with the global conformational change of GPDH. Considering these observations, we claim that a cavity filled with mobile, internal molecules would be a structural outcome that integrates both flexibility of the main intersubunit interface, allowing significant conformational changes to occur, and stability that would preserve the dimeric assembly.

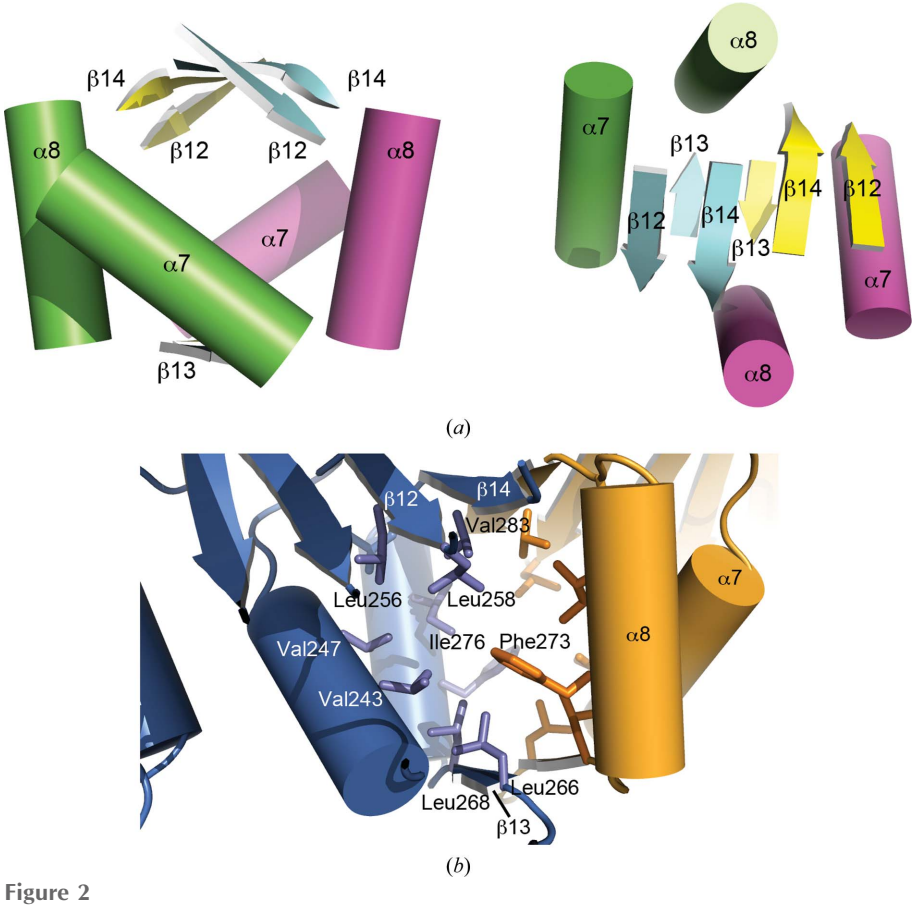

Figure 2
Representation of the regular secondary-structural elements of GPDH that delimitate an internal cavity situated at the main contacting interface between subunits. (*a*) Two orthogonal views of such structural elements (helices and strands from one subunit are shown as green cylinders and cyan arrows, respectively, and those from the other subunit as magenta cylinders and yellow arrows). (*b*) Close-up view of the cavity showing the side chains of the residues facing its lumen. All residues are hydrophobic. Since the cavity exhibits twofold symmetry, only unique residues are indicated for simplicity.

3.3. A global conformational change in GPDH

As indicated above, we have crystallized the binary GPDH–Zn^{2+} complex

(crystal form I) and also performed crystallization trials with the tertiary GPDH–Zn^{2+}–NADH complex, which rendered new monoclinic crystals (crystal form II). Despite the fact that the phased–model difference Fourier map of GPDH calculated using data from these latter crystals did not reveal any electron density assignable to the NADH cofactor, this latter structure (either model 2 or 3), when compared with model 1, reveals the existence of a global conformational change in GPDH similar to that reported for hlADH upon binding the complete cofactor (Eklund *et al.*, 1981). Hence, two distinct conformational states of GPDH were identified: an open state derived from crystal form I (equivalent to the open state of hlADH obtained with the apoenzyme) and a closed state derived from crystal form II (equivalent to the closed state of hlADH obtained with the holoenzyme). The conformational change in hlADH can be described as a rigid-body rotation between the catalytic and cofactor-binding subdomains (Eklund *et al.*, 1981), together with some rearrangements in the 292–299 loop involved in cofactor binding (the β12–β13 connecting loop in GPDH).

Similarly to hlADH, the observed conformational change in GPDH involves relative motion of the catalytic and cofactor-binding subdomains, with helices α9 and 3_{10}-3 acting as a hinge. This movement leads to closure of the cleft between subdomains where the active site is located (Supplementary Movie S1; see below) and can be described as a rigid-body rotation of about 10–12° around an axis between the catalytic and cofactor-binding subdomains. In particular, the N-terminal end of helix α1 and the α10–β16 connecting loop, both from the catalytic subdomain, and helix α5 and the connecting loops between strand β8 and helix α4 and between strands β12 and β13, from the cofactor-binding subdomain, approach the centre of the cleft, narrowing its overall width.

When analyzed in terms of the dimeric assembly, the reorientation of the GPDH subdomains of both subunits results in an in-plane, antiparallel displacement of one β13 strand relative to the other, and also in a change in the relative position of helix α8 from one subunit with respect to the β12–β13 connecting loop from the other subunit (Fig. 3). In contrast, strands β12 and β14 from the extended intersubunit β-sheet remain stationary, probably contributing to the integrity of the dimer as the conformational change occurs, similarly to helices α8. In fact, several intersubunit interactions are identified at both sides of strands β12 and β14: polar interactions between Glu280 and His151 and the carbonyl O atom of Trp287, and stacking interactions between the aromatic rings of the His253 and Phe99 side chains. Interestingly, the imidazole ring of His151 is tightly fixed in position since it bridges between Glu280 from the other subunit and Glu298.

Normal-mode analyses of GPDH with the *ElNémo* web server (Suhre & Sanejouand, 2004) reveals that a single normal mode (the second normal mode for a single subunit and the first normal mode for the dimer) reproduces a conformational transition between an open and a closed conformation of the enzyme in both directions (open →closed and closed→open), in

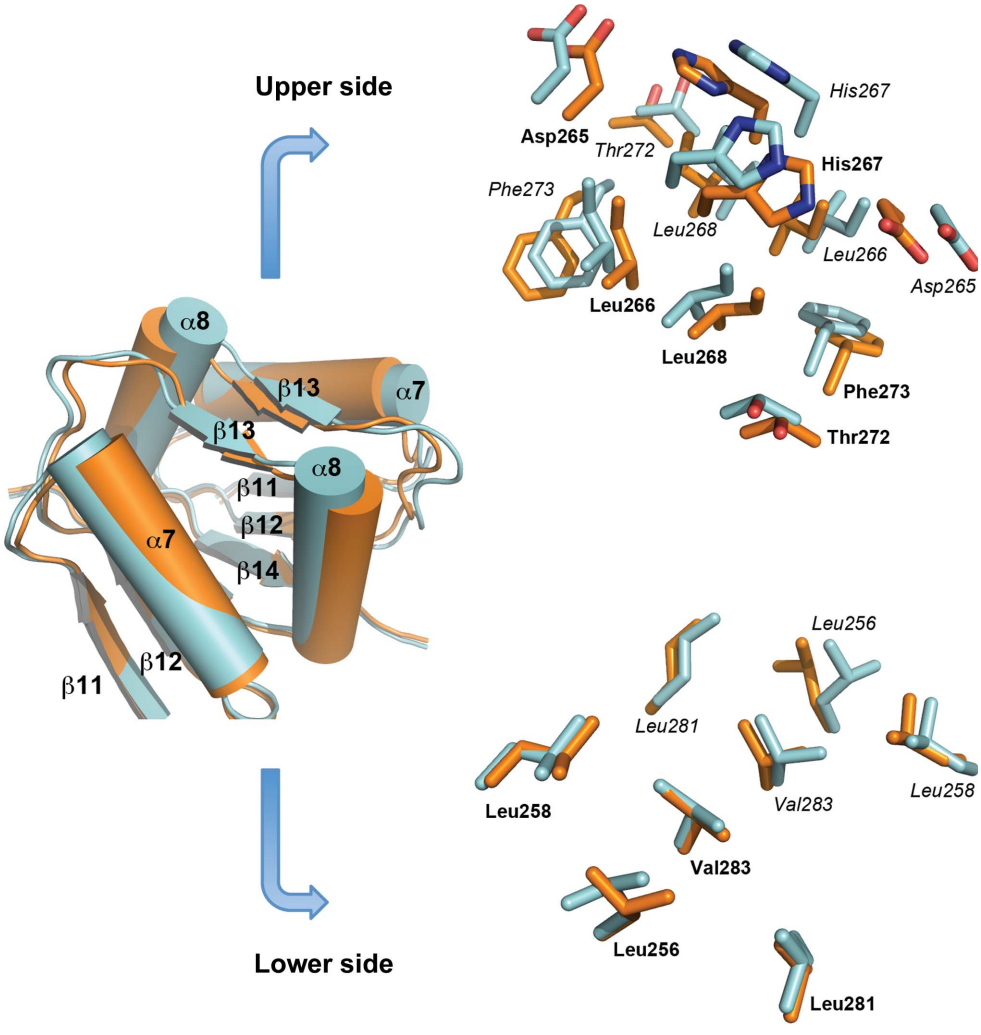

Figure 3
Conformational differences at the intersubunit interface between the closed and open states of GPDH. The global conformational change of GPDH between the open (orange with labels in bold) and closed (cyan with labels in italics) states involves displacements of strands β13 and helices α7 and α8 in the intersubunit region of GPDH, precisely where the hydrophobic cavity is located. Whereas residues facing the upper side of the cavity undergo these displacements (upper part), those on the lower side are not affected (lower part). See the text for details.

which the crystal structures of GPDH would be snapshots lying along the pathway connecting such conformations (Supplementary Movie S2).

As indicated above, residues facing the internal cavity of GPDH participate in the global conformational change. The observed antiparallel displacement of strands β13 involves an in-plane translation of the Leu266 and Leu268 side chains within the cavity, whereas the motions affecting helices α8 and the β12–β13 connecting loops involve displacements of the Leu262, Phe273 and Ile276 side chains. As indicated above, these internal displacements of side chains are probably facilitated by the presence of the internal cavity, where solvent molecules may play a role in protein dynamics.

Curiously, supporting evidence for a role of the cavity as a facilitator of the intersubunit conformational change may also come from hlADH. In this case, the observed conformational change has only minor effects on the dimeric assembly of hlADH in the sense that, apart from changes in the orientation of some side chains (Val294, for instance), intersubunit contacting surfaces are not affected by the reorientation of the protein subdomains. Here, the remarkable observation is that, contrary to GPDH, hlADH has no internal cavity but a highly

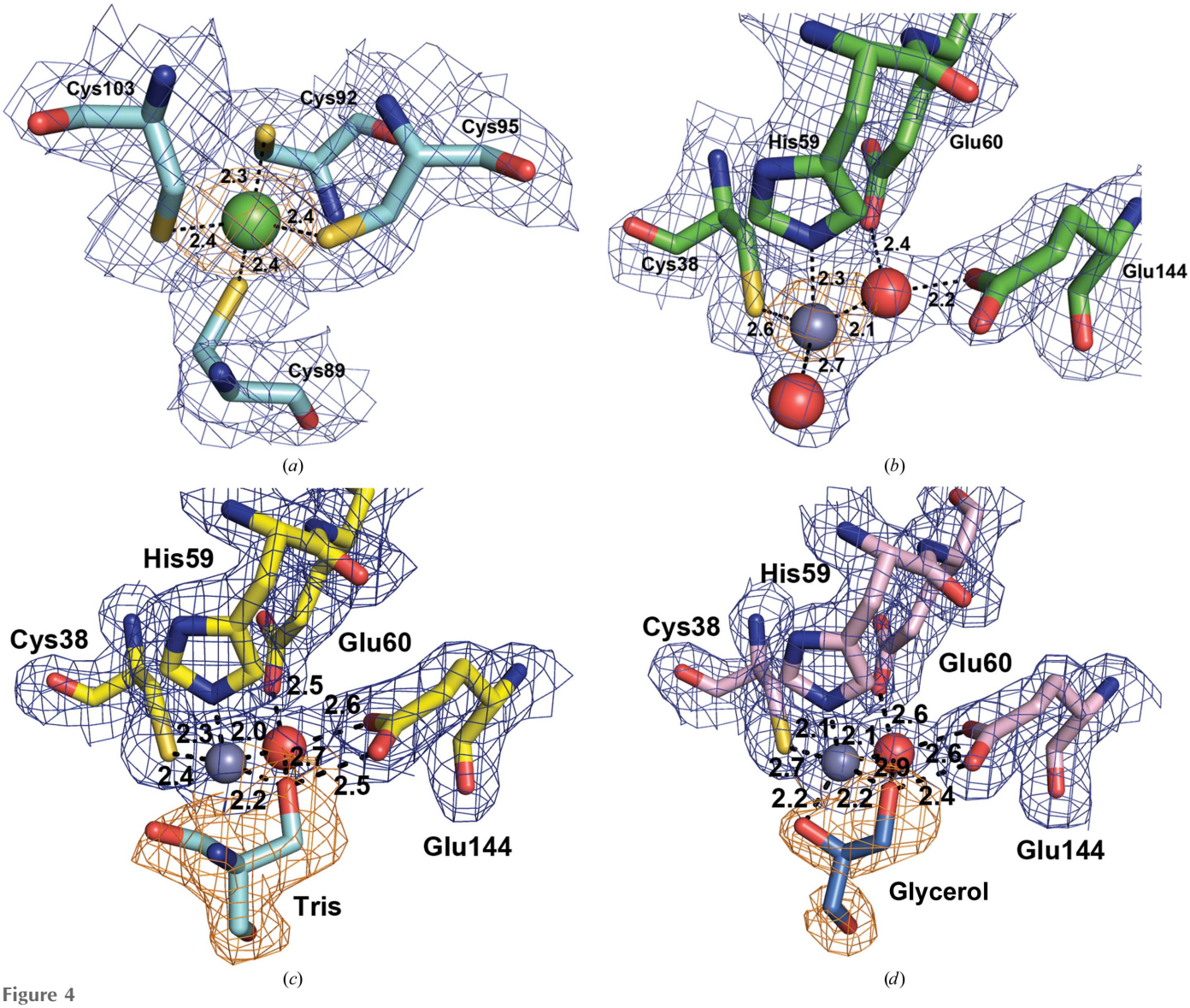

Figure 4
Zinc coordination observed in the different GPDH complexes. (*a*) Structural zinc in the lobe loop. The structural zinc is shown as a green sphere. The electron density for Zn^{2+} (orange) is derived from an anomalous map (5σ level) prepared using data collected at the zinc peak (9.667 keV; 1.28245 Å wavelength) and that for the ligands or the protein is a composite OMIT map (1σ level) calculated with *PHENIX*. (*b*) Catalytic zinc ligands in GPDH pre-incubated with the metal (model 1). The zinc (shown as a grey sphere) is coordinated by interactions with Cys38, His59 (stick representation) and two water molecules (red spheres). The electron-density maps are as in (*a*). (*c*) Catalytic zinc ligands in GPDH with bound Tris. The ligands are Cys38, His59, a conserved water molecule (red sphere) and a hydroxyl group of the Tris molecule. The electron-density map is a composite OMIT map contoured at the 1σ level (for clarity the electron density for Tris is shown as an orange mesh). (*d*) Catalytic zinc ligands in GPDH with bound glycerol. The metal is pentacoordinated by Cys38, His59, a conserved water molecule (red sphere) and two hydroxyl groups of the glycerol molecule. A strong hydrogen bond between the one primary –OH group of glycerol and the carboxylate moiety of Glu144 is represented. In all cases, potential hydrogen bonds are represented as dashed lines. Distances are indicated in Å.

packed hydrophobic core. This hints at a correlation between the presence of an internal cavity (the lack of a tightly packed hydrophobic core) and the existence of local conformational changes at the dimer interface. Obviously, these observations raise numerous questions as to the relationships between the specific catalytic mechanisms of the different ADHs and the distinct conformational degrees of freedom provided by the intersubunit dynamics.

Finally, it is noteworthy that the active site of the closed state of GPDH is observed with no cofactor bound but containing Tris or glycerol instead. This may suggest either that the binding of these molecules induces such a conformational transition in the absence of cofactor or the existence of a conformational equilibrium between the open and closed states in the absence of ligands, which in our studies would probably be shifted by the different crystallization conditions. Although as far as we know this would be a novelty for any MDR enzyme where the scenario is dominated by the induced-fit concept (Plapp, 2010), the conformational selection scenario is a well known phenomenon in enzymatic systems (Changeux, 2013). In fact, it has been proposed that these situations are not mutually incompatible but rather are limiting cases of a more general framework that integrates both phenomena (Hammes *et al.*, 2009).

3.4. Metal ligands

Prior characterization of GPDH revealed the necessity of Zn^{2+} and NAD(H) for the oxidation of galactitol and reduction of D-tagatose 6-phosphate (Esteban-Torres *et al.*, 2012). The metal-binding sites of GPDH that we reported previously revealed two metals to be bound per protein subunit: one Zn^{2+} bound in the structural metal-binding site and another metal located in the catalytic site that we proposed to be a nickel ion scavenged from the purification medium (Esteban-Torres *et al.*, 2012). Now, new crystals of GPDH incubated with Zn^{2+} have permitted the unambiguous identification of the two metals as Zn^{2+}, as revealed by X-ray energy scans and also from anomalous difference maps calculated using data recorded at the Zn peak (9.667 keV; Fig. 4).

The structural zinc ion in all of the structures reported here is located in the lobe loop of the catalytic domain (residues 89–103), where it is coordinated by four cysteine residues (Cys89, Cys92, Cys95 and Cys103) with a tetrahedral geometry (Fig. 4*a*). In this type of coordination where Zn^{2+} forms four strong bonds to cysteine residues the metal does not normally dissociate under biological conditions (Harding *et al.*, 2010), usually playing a role in stabilization of the tertiary structure. This structural metal is also observed in the crystal structures of the close homologues the L-threonine dehydrogenases from *P. horikoshii* (Ishikawa *et al.*, 2007) and from *T. thermophilus* (PDB entry 2dfv) and whitefly ketose reductase (Banfield *et al.*, 2001), but not in hSDH (Pauly *et al.*, 2003), sheep liver sorbitol dehydrogenase (Yennawar *et al.*, 2011) or L-threonine dehydrogenase from *T. kodakaraensis* (Bowyer *et al.*, 2009). This variability in the structural metal-binding site correlates well with the variation in the total zinc content observed in general for other more distant ADHs (Bogin *et al.*, 1997; Korkhin *et al.*, 1998; Sulzenbacher, Alvarez *et al.*, 2004).

Although the structure of GPDH determined from crystals of form I (model 1) reveals a Zn^{2+} in each catalytic site, the low metal occupancy deduced from *B*-factor analysis (an overall Zn^{2+} *B* factor of 125 Å^2 *versus* an overall ligand *B* factor of 63 Å^2) makes the geometry of metal coordination not as reliable as those determined from GPDH models 2 or 3, in which full metal occupancy was observed (model 2, overall Zn^{2+} *B* factor of 27 Å^2 *versus* overall ligand *B* factor of 18 Å^2; model 3, overall Zn^{2+} *B* factor of 20 Å^2 *versus* overall ligand *B* factor of 25 Å^2). Nonetheless, it can be easily ascertained in model 1 that the metal is coordinated by Cys38, His59 and two water molecules (Fig. 4*b*).

Unexpectedly, a different metal coordination is observed for each of the GPDH models from crystal form II (models 2 and 3), which results from the presence of different polyols in the active site that are ligands of the zinc: while a Tris molecule is identified in the active site in model 2, a glycerol is observed in model 3. Most probably, these complexes resulted from the different incubation times of GPDH crystals in the cryoprotectant solution. Thus, short times (∼5–10 s) yielded GPDH crystals with Tris in the active site and longer times (2–3 min) led to the replacement of the Tris molecules by glycerols. In this regard, the rather weak electron density for the amine group of Tris may indicate partial exchange of the molecules. Since glycerol is structurally analogous to the catalytically relevant region of galactitol 1-phosphate, the complex may reveal interactions that most probably occur between GPDH and LG1P.

In model 2 of GPDH the catalytic zinc is coordinated by residues Cys38 and His59, a water molecule and the OH1 hydroxyl of the Tris molecule (Fig. 4*c*). In model 3, however, the zinc is pentacoordinated by Cys38, His59, a water molecule and the OH1 and OH2 hydroxyls of glycerol. The shape of the coordination is a distorted tetragonal pyramid (Fig. 4*d*) typical of pentacoordination (Harding *et al.*, 2010). In this case, the most distorted angle is observed for $N^{\varepsilon 2}$—Zn^{2+}—O(OH1), most probably owing to the formation of an additional interaction: a strong hydrogen bond to the $O^{\varepsilon 2}$ atom of Glu144 (a distance of 2.4 Å). Interestingly, the primary OH1 hydroxyl groups of Tris or glycerol are at a hydrogen-bonding distance from the abovementioned water molecule; hence, the corresponding interaction may contribute to ligand binding. On the contrary, hydroxyl group OH2 (equivalent to the hydroxyl group of LG1P undergoing reaction) exclusively interacts with the metal.

We believe that these latter structural results are remarkable in several aspects: firstly, the existence of the interaction between OH1 and the Glu144 side chain shows that this residue is an essential element of PDH-specific substrate recognition and catalysis. This idea was anticipated almost thirty years ago by Eklund *et al.* (1985) for a model of SDH and is here validated for the first time with a polyol molecule within the active site. Secondly, the structure of bound glycerol supports the binding mode of sorbitol by human SDH, as proposed by Pauly *et al.* (2003), insofar as the C1 and C2 O

Table 2
Kinetic parameters for wild-type GPDH and single-point variants.

Variant	Substrate	K_m† (m*M*)	k_{cat} (s^{-1})	k_{cat}/K_m (s^{-1} M^{-1})
Wild-type	Galactitol‡	26 ± 4	37	1400
Wild-type	LG1P	0.16 ± 0.03	8800	55.0×10^6
Wild-type	DT6P‡	1.00 ± 0.05	19500	19.5×10^6
Ser40Ala	LG1P	0.14 ± 0.01	1500	10.7×10^6
Asp41Asn	LG1P	0.17 ± 0.08	250	1.5×10^6
Arg44Thr	LG1P	0.15 ± 0.01	170	1.1×10^6
Arg44Tyr	LG1P	0.033 ± 0.001	1700	51.5×10^6
His51Ala	LG1P	0.17 ± 0.01	2500	14.7×10^6
Tyr106Ala	LG1P	0.20 ± 0.02	3000	15.0×10^6
Arg112Ala	LG1P	0.09 ± 0.01	2700	30.0×10^6
Met288Arg	LG1P	0.23 ± 0.01	1200	5.2×10^6

† The values correspond to apparent values of K_m. ‡ The experimental conditions used for the assays have been described previously (Esteban-Torres *et al.*, 2012). No activity with up to 100 m*M* DG1P and up to 100 µg ml^{-1} GPDH was observed with the wild-type enzyme and with all variants, respectively.

atoms of sorbitol would coordinate to the zinc ion, leading to a pentacoordinated intermediate. Thirdly, this complex with glycerol is, as far as we know, the first PDH structure to reveal a pentacoordinated Zn^{2+} involving a substrate-analogue polyol that directly participates in metal coordination. In this regard, the crystal structure of human SDH complexed with NADH and the inhibitor CP-166,572 (Pauly *et al.*, 2003; PDB entry 1pl6) also reveals a pentacoordinated Zn^{2+}, although this inhibitor is not a polyol. Furthermore, among the ADHs the only structures that present a pentacoordinated zinc are the binary complex between hlADH and 1,10-phenanthroline (Boiwe & Brändén, 1977), which is not an alcohol, and two other crystal structures (*Homo sapiens* ADH3; PDB entries 1mc5 and 1teh; Sanghani *et al.*, 2002; Yang *et al.*, 1997), in which one Zn^{2+} coordination is established with a water molecule at distances around 3 Å that markedly depart from the average metal–water atom distance derived from the Cambridge Structural Database of 2.09 ± 0.05 Å (Harding *et al.*, 2010).

3.5. Further analysis of the GPDH active site

The structures of GPDH with Tris or glycerol within the active site reveal features that may be relevant to the wider MDR superfamily, in particular aspects related to the pair of acidic residues close to the zinc centre (Glu60 and Glu144 in GPDH). The acidic residue Glu144 is conserved among the PDHs (Jeffery & Jörnvall, 1988) and is not a ligand of the Zn^{2+}, but coordinates the metal *via* a water molecule whose conserved character in PDHs [human (Pauly *et al.*, 2003) and sheep (Yennawar *et al.*, 2011) sorbitol dehydrogenases and whitefly ketose reductase (Banfield *et al.*, 2001)] suggests that it may play a role in catalysis (Klimacek *et al.*, 2007). In GPDH this solvent molecule also interacts with the accompanying acidic residue Glu60, which similarly to Glu144 does not coordinate the Zn^{2+}. The role of Glu60 in catalysis in MDR enzymes in general, and in PDHs in particular, is not clear, although it has been proposed that it may coordinate the Zn^{2+} throughout the catalytic cycle (Ryde, 1995). In agreement with this, Glu60 coordinates the Zn^{2+} in sheep sorbitol dehydrogenase (Yennawar *et al.*, 2011) and whitefly ketose reductase (Banfield *et al.*, 2001). On the other hand, in human SDH it is a ligand of the Zn^{2+} when the enzyme is unliganded (PDB entry 1pl7) or has NAD^+ bound (PDB entry 1pl8), but not when the enzyme is complexed with NADH and the inhibitor CP-166,572 (PDB entry 1pl6). Altogether, this variability in Glu60 metal coordination is consistent with dynamic zinc-coordination ligand exchange during catalysis (Baker *et al.*, 2009; Plapp, 2010). In this regard, the results of recent, thorough analyses of Zn^{2+} coordination in ADHs (including PDHs) from the MDR superfamily (Auld & Bergman, 2008; Raj *et al.*, 2014) are also consistent with this variability.

Another residue that is strictly conserved in all GPDH homologues, and strongly conserved in the MDR superfamily, situated close to the zinc centre is Asp41. No specific role has been assigned to this amino acid in PDHs, although it has been well studied in yeast ADH (Ganzhorn & Plapp, 1988). In GPDH, the carboxyl group of Asp41 interacts with the guanidinium moiety of Arg44 and also with two internal, highly ordered water molecules that participate in a dense network of hydrogen bonds (Fig. 5). In turn, the Arg44 side chain is at a hydrogen-bonding distance from the hydroxyl group of Ser40. One of the latter water molecules, which is strongly conserved in all structurally characterized PDHs, forms a hydrogen bond to His59. Therefore, it can be thought that Asp41, Arg44 and the latter water molecule may contribute to stabilizing the geometry of the active site. To analyse the roles of these residues in deeper detail, we have prepared several variants resulting from single-point mutations.

Removal of the negative charge of Asp41 in the Asp41Asn variant leads to an enzyme with an unaltered K_m for LG1P (Table 2) but with a dramatically decreased k_{cat} for LG1P oxidation (from 8800 to 250 s^{-1}). Since this amino-acid replacement involves amidation of the carboxylate, it seems reasonable to propose that the ionic character of the side

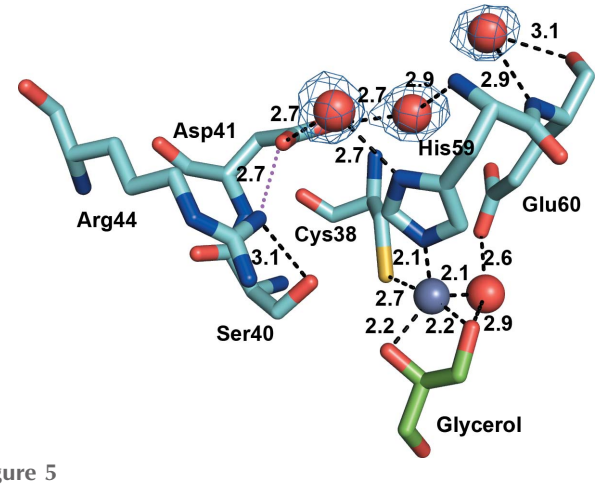

Figure 5
The active site of GPDH. Details of the interactions established between the catalytically important residues Ser40, Asp41 and Arg44 are shown together with the locations of the internal, ordered water molecules (these molecules also appear in model 2). The composite OMIT map around these water molecules (contoured at the 1σ level) is also shown. Potential hydrogen bonds are represented as dashed lines and the ionic interaction between Arg44 and Asp41 is represented as a magenta dotted line. Distances are indicated in Å.

chain is key to its catalytic role. To analyse this aspect in deeper detail, the ionic interaction with Arg44 was removed in the Arg44Thr variant. The effects on the kinetic constants determined for this variant were similar to the Asp41Asn variant (Table 2), revealing the potential relevance of both residues in catalysis. Nonetheless, since Arg44 also interacts with Ser40, which is equivalent to Ser48 in hlADH, which facilitates the deprotonation of the alcohol in this enzyme (Plapp, 2010), the observed effects in GPDH should not be exclusively ascribed to potential destabilization of the active site induced by the loss of the ionic interaction. In fact, our *in silico* analyses of complexes between GPDH and LG1P (or DG1P) strongly support the existence of direct interactions between the guanidinium moiety of Arg44 and both molecules. Most probably, Arg44, together with neighbouring residues, plays a particularly important catalytic role by assisting in the build-up of the correct, extended near-attack conformation of the substrate (see below), which can only be attained with LG1P.

The experimental results obtained with the second variant involving this same residue (Arg44Tyr), where the introduced side chain has a similar length as the parental side chain, may also support such a role. In this case, we observed a smaller effect on turnover number (decreasing from 8800 to 1700 s^{-1}) but a remarkable fivefold reduction in K_m for L1GP (Table 2). This suggests a direct interaction between the introduced side chain and the ground state of the substrate that increases its binding affinity for the enzyme but results in a less catalytically productive conformation that translates into less efficient LG1P oxidation relative to the wild-type enzyme, as was observed previously for the Arg44Thr variant.

Taken together, our results are consistent with the participation of Asp41 (together with the conserved water molecule) in the correct positioning of the His59 side chain; hence, its replacement by Asn could lead to structural rearrangements of the zinc ligands that would affect hydride transfer, thus accounting for the low k_{cat} value that is observed. Conversely, the ionic, buttressing interaction with Arg44 would fix this side chain in such a way as to be properly oriented towards the bound substrate (or DG1P). As a result of the established interactions, a catalytically productive complex can only be achieved with LG1P (see below).

3.6. Biochemical studies

Despite the fact that GPDH has been classically described as a dehydrogenase specific for the oxidation of galactitol 1-phosphate, no direct experimental evidence has been reported showing this specificity. Our previous results on the reverse reaction, namely the reduction of D-tagatose 6-phosphate (DT6P) by GPDH, indicated a 500-fold increase in specific activity (31.50 units mg^{-1}; K_m = 1.00 ± 0.05 m*M*) *versus* the direct reaction of galactitol oxidation (0.06 units mg^{-1}; K_m = 26 ± 4 m*M*) (Esteban-Torres *et al.*, 2012). This is consistent with GPDH being an enzyme with a high specificity towards galactitol 1-phosphate in the direct, oxidation reaction. Nonetheless, a detailed characterization of the Zn^{2+}- and NAD^+-dependent oxidation of galactitol 1-phosphate by GPDH is still required. To this end, we synthesized both LG1P and DG1P. In the enzymatic test system, only LG1P was oxidized when concentrations of less than 0.1 m*M* LG1P and 5 µg ml^{-1} GPDH were used. Furthermore, no activity could be observed with up to 100 m*M* DG1P and 100 µg ml^{-1} GPDH (with the wild-type enzyme or any of the single-point variants). Therefore, our results demonstrate that GPDH exhibits a strict enantioselectivity for LG1P (specific activity of 14.2 units mg^{-1}), which together with our previous results on DT6P reduction unambiguously defines this enzyme as an enantioselective polyol dehydrogenase. Thus, *in vivo*, the enzyme catalyses the reaction LG1P + NAD^+ → DT6P + NADH + H^+.

Comparison of the k_{cat} and K_m values for the LG1P oxidation and DT6P reduction reactions reveals a higher turnover number for DT6P *versus* LG1P, but the approximately sixfold lower K_m for this latter substrate makes the final specificity constant (k_{cat}/K_m) threefold higher for LG1P oxidation than for DT6P reduction.

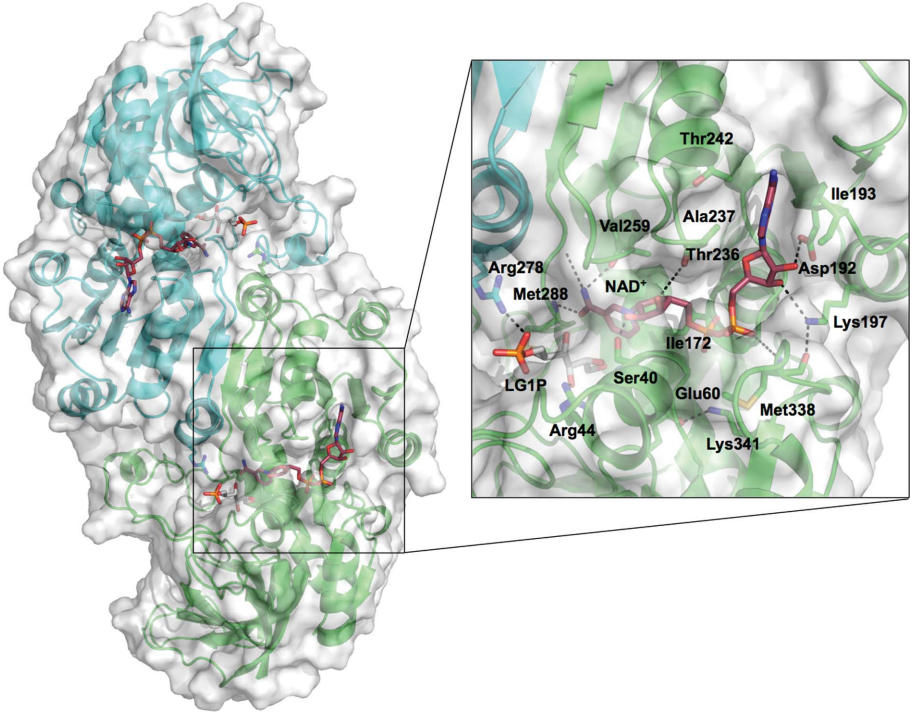

Figure 6
Structural model and close-up view of dimeric GPDH–Zn^{2+} (green and cyan subunits enveloped by a semitransparent surface) in complex with NAD^+ (C atoms in light brown) and LG1P (C atoms in grey). Ligands and labelled active-site residues relevant to the discussion are shown as sticks. Dotted lines represent hydrogen bonds.

Although DG1P could not be oxidized by GPDH, inhibition of LG1P oxidation activity by increasing concentrations of DG1P could be demonstrated in biochemical analysis. From Lineweaver–Burk plots of inhibition kinetics, competitive inhibition by DG1P can be deduced since the plots intersect very closely on the reciprocal velocity axis. In contrast, the K_m for LG1P oxidation is highly affected by the addition of 3 m*M* DG1P, showing an almost sixfold increase (from 0.16 m*M* with no DG1P to 0.92 m*M* with 3 m*M* DG1P), while the reaction velocity is reduced by only 20% (Supplementary Fig. S1; Lineweaver & Burk, 1934).

3.7. NAD$^+$ recognition

Considering our failed attempts to obtain a well defined electron-density map for the cofactor bound to GPDH, we carried out *in silico* studies of the binding mode for NAD$^+$ to the closed state of the enzyme (Fig. 6). In the conservative binding mode proposed, the adenine ring is located in a hydrophobic pocket lined by Ala237, Val239 and Thr242 on one side and Ile193 on the other, whereas the attached ribose establishes hydrogen-bonding interactions with the side chains of Asp192 and Lys197 through its O2′ and O3′ atoms, respectively. This result agrees with the reported structural basis of the specificity for NAD(H) over NADP(H), which resides in the presence of an Asp residue (Asp192 in GPDH) that interacts with the ribose hydroxyl groups (Baker *et al.*, 1992). The diphosphate bridge, in turn, is placed facing the dipole positive end of helix α4 and directly interacts with the NH of Gly39 and the positively charged side chain of Lys341, which is held in place with the assistance of the carboxylate of Glu60 and the carbonyl O atom of Ala80 and Lys197, the amino group of which is fixed in position by the carbonyl O atom of Met338 and the adenosine O3′ hydroxyl. The pyridine ring of the nicotinamide moiety, on the other hand, is surrounded by the hydrophobic side chains of Val148, Ile172 and Val259, with the amide moiety interacting with the carbonyl group of Val259 and the NH of Met288, and the ribose O2′ and O3′ hydroxyl groups engaged in hydrogen bonds to the OH of Ser40 and to the carbonyl O atom of Thr236.

Interestingly, all crystal structures of GPDH reported in this work reveal ordered water molecules interacting with the carbonyl groups of Val259 and Ser286 and additional water molecules in model 1 (which lacks a polyol in the active site) interacting with the main-chain NH of Met288. Hence, the distribution of ordered waters in this region faithfully resembles the predicted position of the amide moiety of the nicotinamide ring bound to GPDH. Moreover, the absence of the latter water molecule interacting with Met288 in models 2 and 3 could be owing to the presence of glycerol or Tris in the active site since the distal parts of these molecules protrude towards the predicted position of the nicotinamide ring, making the simultaneous presence of both cofactor and polyol mutually exclusive.

3.8. GDPH substrate recognition and reaction mechanism

The two conformational states of the GPDH subunits may represent structures relevant to the catalytic mechanism of the enzyme, namely the apoenzyme (open state) and the ternary complex (closed state), as suggested by the structural similarity to hlADH, the isomerization step of which has been described in detail (Sekhar & Plapp, 1990; Kovaleva & Plapp, 2005). Therefore, we propose the following scenario for GPDH: in the absence of any bound ligand an equilibrium would exist between the open and closed states of the enzyme. In both cases the zinc ion is tetracoordinated by two protein side chains (Cys38 and His59) and two water molecules. The required cofactor NAD$^+$ would bind the closed state of the enzyme first (conformational selection model), followed by the binding of LG1P. LG1P binds with both its C5 and C6 O atoms coordinated to the zinc, with the concurrent release of a water molecule: zinc-ligand exchanges would then yield a pentacoordinated metal ion (model 3). Our *in silico* model of the ternary complex (Fig. 7) shows that LG1P stacks in part against the nicotinamide ring, and this is consistent with an ordered mechanism.

The proton transfer from the C5 hydroxyl group of LG1P required for oxidation of LG1P to DT6P demands a base, a role which has been assigned in hSDH (Pauly *et al.*, 2003) and sheep liver SDH (Klimacek *et al.*, 2007) to the water molecule that interacts with Glu60 and Glu144 in GPDH. Based on our structural and

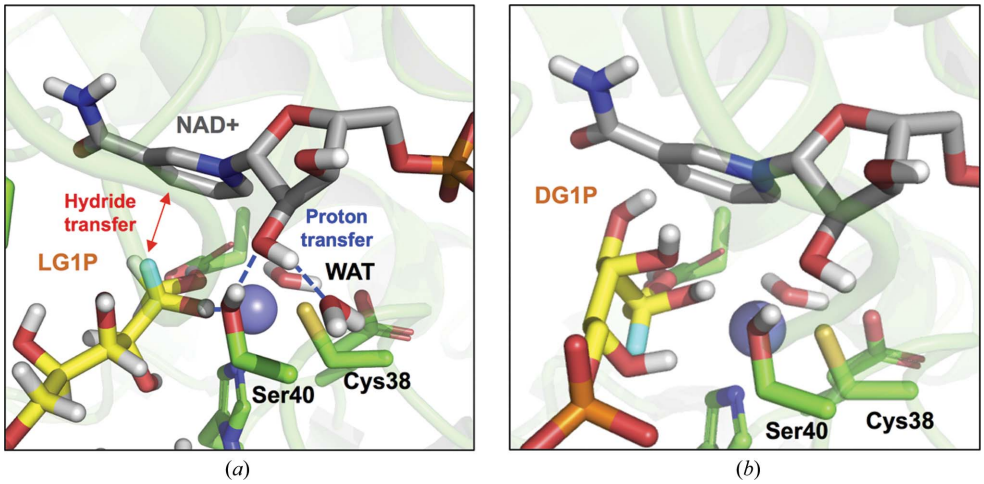

Figure 7
Proposed binding modes for (*a*) LG1P and (*b*) DG1P in the GPDH catalytic site. Note the correct positioning of the C5 H atom (coloured cyan) facing the pyridine C4 atom of NAD$^+$ in the complex with LG1P, at the expected distance from the C4 atom of the pyridine moiety for hydride transfer to occur, and the opposite orientation of the equivalent H atom in DG1P.

functional analyses, we claim that catalysis by GPDH is consistent with the generally accepted mechanism proposed by Eklund *et al.* (1982) (see also Plapp, 2010 for a review). In this scenario, the hydroxyl group of Ser40 in GPDH (Ser or Thr residues systematically appear in this position in PDHs) acts as part of the relay system that transfers the proton of the C5 hydroxyl group to the bulk water. The predicted conformation of bound LG1P indicates that upon Zn^{2+} coordination by the substrate, most likely funnelled by the strong hydrogen bond between the primary C6 hydroxyl group and the carboxylate of Glu144, the orientation of the secondary C5 hydroxyl group is adequate for such a proton transfer exclusively for LG1P. The participation of Ser40 in catalysis can be inferred from the kinetic parameters determined for the Ser40Ala variant: while K_m for LG1P remains essentially unaltered, an important reduction in the turnover number is observed (from 8800 to 1500 s^{-1}; Table 2), which is consistent with the assigned role in abstracting the proton from the C5 hydroxyl group of the substrate. This deprotonation is facilitated by the polarization of the O—H bond by the bound Zn^{2+} ion, which therefore plays the role of a Lewis acid. The evolving negative charge on the secondary alcohol then drives the subsequent transfer of the negatively charged hydride to the positively charged cofactor. This reaction scheme, which is only possible for LG1P, would lead to cofactor reduction and oxidation of the C5 hydroxyl to the keto group of DT6P.

Although according to the proposed substrate-binding mode many residues contribute to the definition of the complete substrate-binding pocket (Cys38, Ser40, Arg44, His51, His59, Tyr106, Phe108, Ser111, Arg112, Glu144, Trp287 and Met288), we observe that two residues, namely Arg44 and Met288, would directly interact with LG1P: Arg44 would interact with the C4 hydroxyl group and Met288 would establish hydrophobic interactions with the C4–C5–C6 backbone atoms of LG1P (Fig. 6). Hence, a role in substrate orientation (that will ultimately lead to enantiomer discrimination) can be predicted for them. The important role of Arg44 in catalysis could be inferred from the two variants discussed above (Arg44Thr and Arg44Tyr), and that of Met288 was checked using the Met288Arg variant, which revealed a drastic decrease in k_{cat} for LG1P oxidation (similar to that observed for the Arg44Thr variant), with K_m remaining unaltered.

The finding that DG1P behaves as a competitive inhibitor of LG1P oxidation supports the view that the configuration of the substrate-binding pocket is compatible with DG1P binding (Fig. 7). However, the predicted interactions established with Zn^{2+}, the Glu144 carboxylate, Arg44 and Met288 would lead to a conformation that is incompatible with both proton and hydride transfer, the former owing to the improper orientation of the secondary C5 hydroxyl group relative to Ser40 and the latter because the C5 H atom would be oriented away from the pyridine ring of the NAD^+ coenzyme. Inhibition of LG1P activity by increasing concentrations of DG1P could be demonstrated in biochemical analysis. From Lineweaver–Burk plots of inhibition kinetics, competitive inhibition by DG1P can be deduced because the intersection of the plots is close on the reciprocal velocity axis. The K_m for LG1P oxidation is highly affected and decreases by almost sixfold on the addition of 3 m*M* DG1P, while the reaction velocity is only reduced by 20% (Supplementary Fig. S1).

We also propose that three residues of the pocket, namely His51, Tyr106 and Arg112, are also important in substrate specificity by playing a bait role for attracting the phosphate group and probably facilitating product release as well. This proposal is supported by the available structural evidence and results from our molecular dynamics simulations (data not shown) revealing that these residues can be oriented towards the solvent (open state) or towards the active site (closed state). The finding that site-directed mutagenesis at these three positions resulted in enzymes that display decreased turnover numbers but K_m values similar to those of the wild-type enzyme (Table 2) appears to support this assigned function. Finally, these same studies also revealed that the Arg278 side chain from one subunit might also be engaged in fixation of the phosphate moiety of the substrate by the other subunit. This finding suggests the existence of 'cross-talk' between subunits which, together with the fact that the global conformational change of GPDH involves the dimer interface, would open the possibility of cooperative effects. These aspects, which as far as we know have not been described for hlADH, are currently under investigation.

Acknowledgements

We thank the ESRF, Grenoble, France and the ALBA synchrotron, Barcelona, Spain for provision of synchrotron-radiation facilities (the ID23-1 and ID29 beamlines at the ESRF and XALOC at ALBA). Financial support to JMM from Ministerio de Educación y Ciencia (BFU2010-17929/BMC) and the Factoría de Cristalización (Consolider-Ingenio-2007), to FG from Ministerio de Economía y Competitividad (SAF2012-39760-C02-02) and Comunidad de Madrid (S2010-BMD-2457) and to GWK from the European Community through the FP7-NMP-2007-SMALL 1 collaborative project ERUDESP is greatly acknowledged.

References

Adams, P. D. *et al.* (2010). *Acta Cryst.* D**66**, 213–221.
Afonine, P. V., Grosse-Kunstleve, R. W., Echols, N., Headd, J. J., Moriarty, N. W., Mustyakimov, M., Terwilliger, T. C., Urzhumtsev, A., Zwart, P. H. & Adams, P. D. (2012). *Acta Cryst.* D**68**, 352–367.
Al-Karadaghi, S., Cedergren-Zeppezauer, E. S., Hovmöller, S., Petratos, K., Terry, H. & Wilson, K. S. (1994). *Acta Cryst.* D**50**, 793–807.
Auld, D. S. & Bergman, T. (2008). *Cell. Mol. Life Sci.* **65**, 3961–3970.
Bae, B., Sullivan, R. P., Zhao, H. & Nair, S. K. (2010). *J. Mol. Biol.* **402**, 230–240.
Baker, P. J., Britton, K. L., Fisher, M., Esclapez, J., Pire, C., Bonete, J., Ferrer, J. & Rice, D. W. (2009). *Proc. Natl Acad. Sci. USA*, **106**, 779–784.
Baker, P. J., Britton, K. L., Rice, D. W., Rob, A. & Stillman, T. J. (1992). *J. Mol. Biol.* **228**, 661–671.
Banfield, M. J., Salvucci, M. E., Baker, E. N. & Smith, C. A. (2001). *J. Mol. Biol.* **306**, 239–250.
Bellamacina, C. R. (1996). *FASEB J.* **11**, 1257–1269.
Bogin, O., Peretz, M. & Burstein, Y. (1997). *Protein Sci.* **6**, 450–458.
Boiwe, T. & Brändén, C.-I. (1977). *Eur. J. Biochem.* **77**, 173–179.

Bowyer, A., Mikolajek, H., Stuart, J. W., Wood, S. P., Jamil, F., Rashid, N., Akhtar, M. & Cooper, J. B. (2009). *J. Struct. Biol.* **168**, 294–304.
Brändén, C.-I. (1965). *Arch. Biochem. Biophys.* **112**, 215–217.
Buckle, A. M., Cramer, P. & Fersht, A. R. (1996). *Biochemistry*, **35**, 4298–4305.
Changeux, J.-P. (2013). *Nature Rev. Mol. Cell Biol.* **14**, 819–829.
Chen, V. B., Arendall, W. B., Headd, J. J., Keedy, D. A., Immormino, R. M., Kapral, G. J., Murray, L. W., Richardson, J. S. & Richardson, D. C. (2010). *Acta Cryst.* D**66**, 12–21.
Cortés Cabrera, Á., Klett, J., Dos Santos, H. G., Perona, A., Gil-Redondo, R., Francis, S. M., Priego, E. M., Gago, F. & Morreale, A. (2012). *J. Chem. Inf. Model.* **52**, 2300–2309.
DeLano, W. L. (2008). *PyMOL*. http://www.pymol.org.
Dundas, J., Ouyang, Z., Tseng, J., Binkowski, A., Turpaz, Y. & Liang, J. (2006). *Nucleic Acids Res.* **34**, W116–W118.
Dworschack, R. T. & Plapp, B. V. (1977). *Biochemistry*, **16**, 2716–2725.
Edwards, K. J., Barton, J. D., Rossjohn, J., Thorn, J. M., Taylor, G. L. & Ollis, D. L. (1996). *Arch. Biochem. Biophys.* **328**, 173–183.
Eklund, H., Horjales, E., Jörnvall, H., Brändén, C.-I. & Jeffery, J. (1985). *Biochemistry*, **24**, 8005–8012.
Eklund, H., Plapp, B. V., Samama, J.-P. & Brändén, C.-I. (1982). *J. Biol. Chem.* **257**, 14349–14358.
Eklund, H. & Ramaswamy, S. (2008). *Cell. Mol. Life Sci.* **65**, 3907–3917.
Eklund, H., Samama, J.-P., Wallén, L., Brändén, C.-I., Akeson, A. & Jones, T. A. (1981). *J. Mol. Biol.* **146**, 561–587.
Emsley, P., Lohkamp, B., Scott, W. G. & Cowtan, K. (2010). *Acta Cryst.* D**66**, 486–501.
Englander, S. W. & Kallenbach, N. R. (1983). *Q. Rev. Biophys.* **16**, 521–655.
Eriksson, A. E., Baase, W. A., Zhang, X. J., Heinz, D. W., Blaber, M., Baldwin, E. P. & Matthews, B. W. (1992). *Science*, **255**, 178–183.
Esposito, L., Sica, F., Raia, C. A., Giordano, A., Rossi, M., Mazzarella, L. & Zagari, A. (2002). *J. Mol. Biol.* **318**, 463–477.
Esteban-Torres, M., Álvarez, Y., Acebrón, I., de las Rivas, B., Muñoz, R., Kohring, G.-W., Roa, A. M., Sobrino, M. & Mancheño, J. M. (2012). *FEBS Lett.* **586**, 3127–3133.
Evans, P. R. (2011). *Acta Cryst.* D**67**, 282–292.
Fan, F. & Plapp, B. V. (1999). *Arch. Biochem. Biophys.* **367**, 240–249.
Ganzhorn, A. J. & Plapp, B. V. (1988). *J. Biol. Chem.* **263**, 5446–5454.
Guy, J. E., Isupov, M. N. & Littlechild, J. A. (2003). *J. Mol. Biol.* **331**, 1041–1051.
Hammes, G. G., Chang, Y.-C. & Oas, T. G. (2009). *Proc. Natl Acad. Sci. USA*, **106**, 13737–13741.
Harding, M. M., Nowicki, M. W. & Walkinshaw, M. D. (2010). *Crystallogr. Rev.* **16**, 247–302.
Holm, L. & Sander, C. (1995). *Trends Biochem. Sci.* **20**, 478–480.
Ishikawa, K., Higashi, N., Nakamura, T., Matsuura, T. & Nakagawa, A. (2007). *J. Mol. Biol.* **366**, 857–867.
Jackson, S. E., Moracci, M., elMasry, N., Johnson, C. M. & Fersht, A. R. (1993). *Biochemistry*, **32**, 11259–11269.
Jeffery, J. & Jörnvall, H. (1988). *Adv. Enzymol. Relat. Areas Mol. Biol.* **61**, 47–106.
Kabsch, W. (2010). *Acta Cryst.* D**66**, 125–132.
Kleifeld, O. (2003). *Protein Sci.* **12**, 468–479.
Klimacek, M., Hellmer, H. & Nidetzky, B. (2007). *Biochem. J.* **404**, 421–429.
Korkhin, Y., Kalb(Gilboa), A. J., Peretz, M., Bogin, O., Burstein, Y. & Frolow, F. (1998). *J. Mol. Biol.* **278**, 967–981.
Kovaleva, E. G. & Plapp, B. V. (2005). *Biochemistry*, **44**, 12797–12808.
Lineweaver, H. & Burk, D. (1934). *J. Am. Chem. Soc.* **56**, 658–666.
Makinen, M. W. & Yim, M. B. (1981). *Proc. Natl Acad. Sci. USA*, **78**, 6221–6225.
Matthews, B. W., Morton, A. G., Dahlquist, F. W., Ernst, J. A., Clubb, R. T., Zhou, H.-X., Gronenborn, A. M. & Clore, G. M. (1995). *Science*, **270**, 1847–1849.
McCoy, A. J., Grosse-Kunstleve, R. W., Adams, P. D., Winn, M. D., Storoni, L. C. & Read, R. J. (2007). *J. Appl. Cryst.* **40**, 658–674.
Nobelmann, B. & Lengeler, J. W. (1995). *Biochim. Biophys. Acta*, **1262**, 69–72.
Pauly, T. A. *et al.* (2003). *Structure*, **11**, 1071–1085.
Pennacchio, A., Esposito, L., Zagari, A., Rossi, M. & Raia, C. A. (2009). *Extremophiles*, **13**, 751–761.
Persson, B., Hedlund, J. & Jörnvall, H. (2008). *Cell. Mol. Life Sci.* **65**, 3879–3894.
Persson, B., Zigler, J. S. & Jörnvall, H. (1994). *Eur. J. Biochem.* **226**, 15–22.
Plapp, B. V. (2010). *Arch. Biochem. Biophys.* **493**, 3–12.
Raj, S. B., Ramaswamy, S. & Plapp, B. V. (2014). *Biochemistry*, **53**, 5791–5803.
Riveros-Rosas, H., Julián-Sánchez, A., Villalobos-Molina, R., Pardo, J. P. & Piña, E. (2003). *Eur. J. Biochem.* **270**, 3309–3334.
Ryde, U. (1995). *Protein Sci.* **4**, 1124–1132.
Sanghani, P. C., Bosron, W. F. & Hurley, T. D. (2002). *Biochemistry*, **41**, 15189–15194.
Sekhar, V. C. & Plapp, B. V. (1990). *Biochemistry*, **29**, 4289–4295.
Shimomura, Y., Kakuta, Y. & Fukuyama, K. (2003). *J. Bacteriol.* **185**, 4211–4218.
Smith, P. K., Krohn, R. I., Hermanson, G. T., Mallia, A. K., Gartner, F. H., Provenzano, M. D., Fujimoto, E. K., Goeke, N. M., Olson, B. J. & Klenk, D. C. (1985). *Anal. Biochem.* **150**, 76–85.
Suhre, K. & Sanejouand, Y.-H. (2004). *Nucleic Acids Res.* **32**, W610–W614.
Sulzenbacher, G., Alvarez, K., van den Heuvel, R. H., Versluis, C., Spinelli, S., Campanacci, V., Valencia, C., Cambillau, C., Eklund, H. & Tegoni, M. (2004). *J. Mol. Biol.* **342**, 489–502.
Sulzenbacher, G., Roig-Zamboni, V., Pagot, F., Grisel, S., Salomoni, A., Valencia, C., Campanacci, V., Vincentelli, R., Tegoni, M., Eklund, H. & Cambillau, C. (2004). *Acta Cryst.* D**60**, 1855–1862.
Winn, M. D. *et al.* (2011). *Acta Cryst.* D**67**, 235–242.
Wolfenden, R. & Radzicka, A. (1994). *Science*, **265**, 936–937.
Yang, Z.-N., Bosron, W. F. & Hurley, T. D. (1997). *J. Mol. Biol.* **265**, 330–343.
Yennawar, H., Møller, M., Gillilan, R. & Yennawar, N. (2011). *Acta Cryst.* D**67**, 440–446.
Yu, B., Blaber, M., Gronenborn, A. M., Clore, G. M. & Caspar, D. L. D. (1999). *Proc. Natl Acad. Sci. USA*, **96**, 103–108.